From snow accumulation to snow depth distributions by quantifying meteoric ice fractions in the Weddell Sea

Stefanie Arndt[1], Nina Maaß[1,2], Leonard Rossmann[1], Marcel Nicolaus[1]

[1]Alfred-Wegener-Institut Helmholtz-Zentrum für Polar- und Meeresforschung, 27570 Bremerhaven, Germany
[2] Center for Earth System Research and Sustainability, University of Hamburg, 20146 Hamburg, Germany

Correspondence to: Stefanie Arndt (stefanie.arndt@awi.de)

Abstract. A year-round snow cover is a characteristic of the entire Antarctic sea ice cover, which has significant implications for the energy and mass budgets of sea ice, e.g., by preventing surface melt in summer and enhancing sea ice growth through extensive snow ice formation. However, substantial observational gaps in the seasonal cycle of Antarctic sea ice and its snow cover limit the understanding of important processes in the ice-covered Southern Ocean. They also introduce large uncertainties in satellite remote sensing applications and climate studies.

Here we present results from 10 years of autonomous snow observations from Snow Buoys in the Weddell Sea. To distinguish between actual snow depth and potential snow ice thickness within the accumulated snowpack, a one-dimensional thermodynamic sea ice model is applied along the drift trajectories of the buoys. The results show that potential snow ice formation, with an average maximum thickness of 35 cm, was detected along 41% of the total track length of the analyzed Snow Buoy tracks, which corresponds to about one quarter of the snow accumulation. In addition, we simulate the evolution of internal snow properties along the drift trajectories with the more complex SNOWPACK model, which results in superimposed ice thicknesses between 0 and 16 cm. These estimates will provide an important reference dataset for both snow depth and meteoric ice rates in the Southern Ocean.

Short summary. Antarctic sea ice maintains year-round snow cover, crucial for its energy and mass budgets. Despite its significance, snow depth remains poorly understood. Over the last decades, Snow Buoys have been deployed extensively on the sea ice to measure snow accumulation but not actual depth due to snow transformation into meteoric ice. Therefore, in this study, we utilize sea ice and snow models to estimate meteoric ice fractions in order to calculate actual snow depth in the Weddell Sea.

1 Introduction

The role of the snow cover is particularly intriguing for the understanding of sea ice mass budget in the Southern Ocean, as Antarctic snow cover survives potential summer melt and persists during most of the year (Massom et al., 2001). The low thermal conductivity makes snow an effective insulator, and thus dampens the thermodynamic ice growth at the bottom

30   (Calonne et al., 2011; Sturm et al., 1997). It also contributes to ice growth from the top through the formation of meteoric ice (Eicken et al., 1994). Snow-to-ice conversion processes, i.e., snow ice and superimposed ice formation, are instrumental in comprehending this complex system. Snow ice results from the submergence of the ice surface beneath the seawater level, facilitated by heavy snow loads (e.g., Eicken et al., 1994; Tian et al., 2020). Subsequent flooding and refreezing of the snow/water mixture result in the creation of this unique ice form, a process that is particularly pronounced during the winter

35   months. In contrast, the formation of superimposed ice is driven by internal melting within the snowpack during summer as snowmelt water percolates downward and refreezes at the snow/ice interface (Ackley et al., 2008; Nicolaus et al., 2009; Haas and Eicken, 2001; Arndt et al., 2021).

As such, Arndt (2022) and Arndt et al. (2021) outline mean snow ice thicknesses of 0.18 ± 0.18 m in the southeastern Weddell Sea and 0.22 ± 0.22 m in the northwestern Weddell Sea during late summer. In the Ross Sea, Kawamura et al. (1997) observed

40   similar ratios of snow ice to total sea ice thickness, with 22% for first-year ice and 10% for multi-year ice. Conversely, Ackley et al. (2020) reported a snow ice thicknesses of 30 to 35 cm in the Amundsen Sea, attributed to intense bottom melt driven by high ocean heat fluxes and low ice concentration. For the superimposed ice layer, Haas et al. (2001) documented varying thicknesses, with 0.08 ± 0.06 m in the northwestern Weddell Sea, 0.10 ± 0.05 m in the Amundsen Sea, and 0.12 ± 0.07 cm in the Bellingshausen Sea.

45   In addition to its direct effects, snow also hampers the interpretation and retrieval of sea ice parameters, including thickness and volume of sea ice observed using in-situ and with satellite remote sensing. The conversion of either ice draft, measured by means of upward looking sonars, or ice freeboard, measured by means of satellite altimetry (Ricker et al., 2015; Fons and Kurtz, 2019; Kwok et al., 2020), into ice thickness, depends heavily on reliable snow depth and density data. As the ratio of snow load to ice thickness is particularly high for Antarctic sea ice, the snow cover has a significant effect on the freeboard of

50   Antarctic sea ice (Worby et al., 2008). Consequently, the estimation of ice thickness is particularly reliant on the conversion of freeboard to thickness, resulting in significant uncertainty in Antarctic sea ice thickness retrievals (Paul et al., 2018; Kwok and Kacimi, 2018; Schwegmann et al., 2016).

Despite the fact, that snow depth on sea ice is such an essential state variable of the polar climate system, it is yet one of the least known parameters for Antarctic sea ice (Webster et al., 2018). However, attempts have been made to describe it at

55   different spatial scales. Therefore, it is imperative to distinguish between the terminologies of snow accumulation and snow depth since the two may not always correspond due to the various snow conversion processes outlined above. Snow accumulation refers to all the snow that has fallen or has been redistributed by wind at a certain location during a specified period of time. Snow depth (or thickness), in turn, describes the actual amount of snow present at a specific location and time, which results from the difference between snow accumulation and the thickness of meteoric ice formed up to that point in

60   time. In contrast, snow ablation refers to the process of snow (height) loss due to factors such as melting, metamorphism, sublimation, or other forms of erosion.

Measurements with an automated snow depth probe (MagnaProbe), for example, can be used to determine snow depth at a certain point in time at a certain location (Sturm and Holmgren, 2018). To extend these point measurements, in particular, to larger temporal scales, Snow Buoys have been developed. These are autonomous measuring systems deployed on the sea ice

65   and measure, among other things, hourly snow accumulation rates along the drift and transmit them via satellite link (Nicolaus et al., 2021). However, these ice-tethered platforms cannot describe the potential conversion processes of snow into meteoric ice at the snow/ice interface. As a result, snow accumulation from Snow Buoys cannot be taken as a direct measure of snow depth.

To bridge this gap and finally get a first approximation of snow depth distributions in the Weddell Sea for different regions

70   and seasons, this study uses a simple thermodynamic sea ice model to quantify potential snow ice formation along the trajectories of Snow Buoys in the Weddell Sea over the last decade. In addition, the snow model SNOWPACK is utilized to estimate superimposed ice formation along the same trajectories. The resulting snow and superimposed layer thicknesses are validated with in-situ observations in the southeastern and northwestern Weddell Sea in recent years.

Given that different ice classes experience different contributions from these processes, the reduction in uncertainties varies

75   across the Antarctic sea ice cover. Nevertheless, the results presented reveal distinct variations between regions and seasons, providing a pathway towards improved snow depth datasets. This improvement, in turn, has the potential to reduce uncertainties in sea ice thickness data products derived from satellite remote sensing and sea ice modelling applications.

2 Data and methods
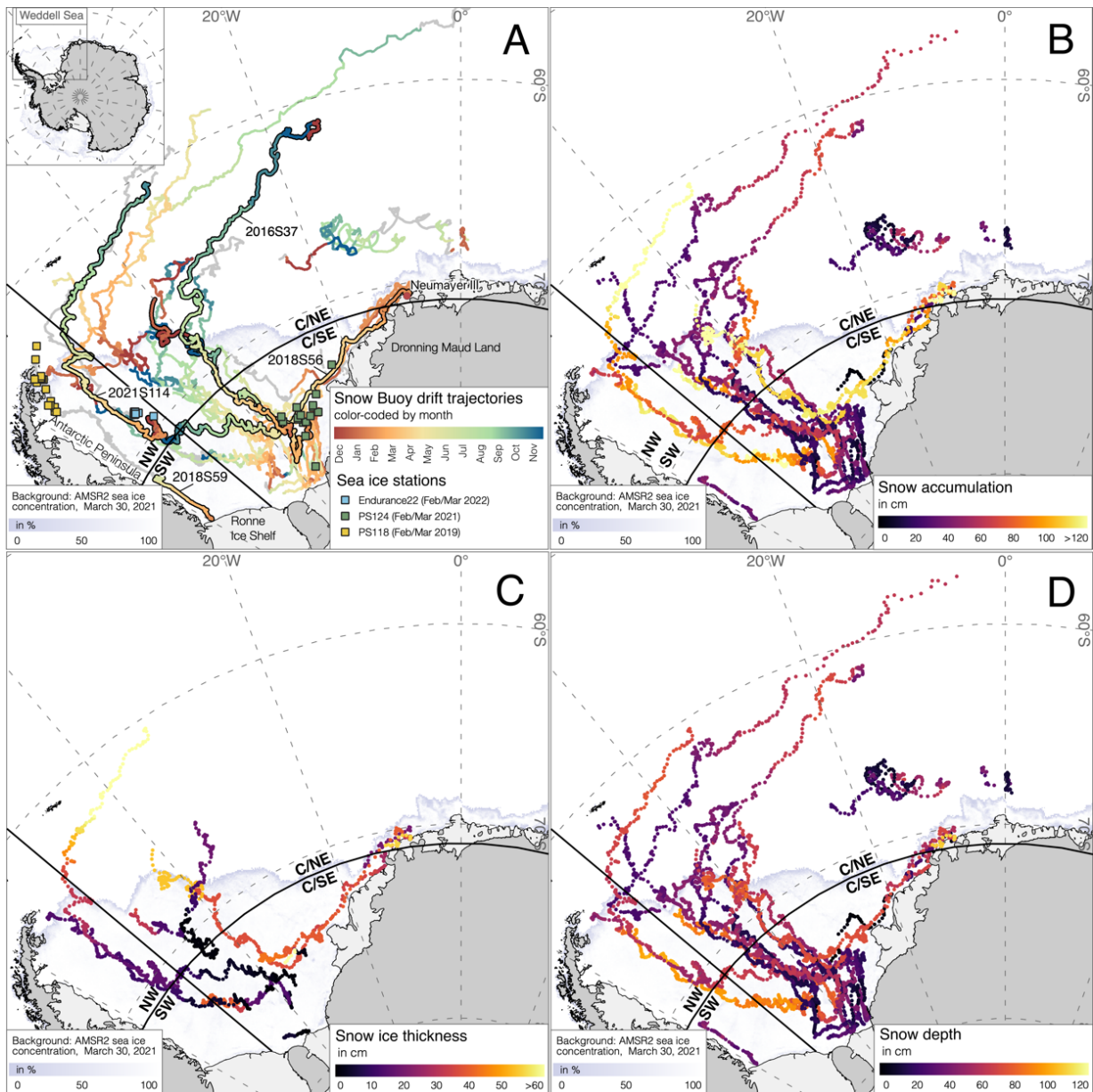
Figure 1. A Map of all Snow Buoy drift trajectories since 2013 in the Weddell Sea. The trajectories are color-coded by month for the time of valid snow accumulation data. Further buoy drifts without valid snow accumulation data are marked in gray. The black-margined trajectories highlight the paths of the Snow Buoys 2016S37, 2018S56, 2018S59 and 2021S114. They are examples of the defined drift patterns in the Weddell Sea (e.g., Chapter 3.1). Colored squares mark additional ice station data from the given expeditions that complement the Snow Buoy data. **B** Snow accumulation measured from the Snow Buoys along

85 their drift trajectory. **C** Estimated snow ice thickness from the one-dimensional thermodynamic ice growth model and **D** resulting calculated snow depth. For all panels: Solid black lines mark the four separated regions: southwestern (SW), northwestern (NW), central/ southeastern (C/SE), central/ northeastern (C/NE) Weddell Sea. Background: AMSR2 sea ice concentration from March 30, 2021 (Spreen et al., 2008).

2.1 Study area

90 The Weddell Sea features a distinctive large-scale cyclonic circulation pattern, the Weddell Gyre, which is driven primarily by mean atmospheric geostrophic forcing (Vernet et al., 2019). This circulation, combined with wind stress, influences surface ocean currents, resulting in an inflow of sea ice in the eastern region and an outflow in the northwest. Within this drift, parts of the sea ice cover survive the summer melt and eventually become second year ice. Drift dynamics, coupled with the pronounced seasonality of the ice cover, contribute to the predominance of seasonal ice in the eastern Weddell Sea and promote

95 the formation of polynyas, particularly along the coast of the Ekström Ice Shelf and the Filchner-Ronne Ice Shelf (e.g., Paul et al., 2015). As a result, sea ice reaches maximum thicknesses of up to 1.5 m near the coast of Dronning Maud Land, while second year ice in the southwestern and western regions can reach thicknesses exceeding 3 m, representing some of the thickest sea ice in the Southern Ocean (Haas et al., 2008; Harms et al., 2001).

For the purposes of this study, the Weddell Sea has been divided into four regions (Figure 1A). The southwestern Weddell Sea

100 (SW) includes the compact perennial sea ice, located south of 71°S and west of 50°W. The northwestern Weddell Sea (NW) includes the predominantly perennial sea ice and the western marginal ice zone, located north of 71°S and west of 50°W. The central and southeastern Weddell Sea (C/SE) corresponds to the highly dynamic, predominantly seasonal sea ice south of 71°S and east of 50°W. Finally, the central and northeastern Weddell Sea represents the marginal sea ice zone, consisting of both seasonal and perennial sea ice, north of 71°S and east of 50°W.

2.2 Snow Buoys

Snow Buoys are autonomous measuring systems hourly recording snow accumulation under four ultra-sonic sensors as well as air temperature and barometric air pressure. Given the height of the sensor mast, a maximum snow accumulation of 1.50 m can be recorded. The systems are deployed on sea ice and transmit their data via satellite connection. For more technical details, see Nicolaus et al. (2021). For this study, all Snow Buoys deployed between 2013 and 2022 on drifting pack ice in the Weddell

110 Sea (27 buoys) or on the fast ice in Atka Bay (9 buoys), close to the German overwintering base Neumayer Station III (Arndt et al., 2020), are considered (Figure 1A). As the Snow Buoys in the Weddell Sea were deployed during ship-based expeditions, which usually take place in austral summer, most time series start between December and February. All snow accumulation values of the individual Snow Buoys are presented as a daily average of all four ultra-sonic sensors. Monthly accumulation (ablation) rates are then calculated as the sum of the positive (negative) changes in these daily values over each month.

115   Here we use the buoy's names, as introduced in Nicolaus et al. (2021), consisting of the deployment year, the buoy type 'S', and a serial counter (Grosfeld et al., 2015).

    For the analysis of the Snow Buoy data, it needs to be taken into account that most buoys were deployed on sea ice either during or towards the end of summer, making the ice floes at least one year old during the deployments. As a result, the mean snow depths primarily represent data from second-year sea ice. Additionally, some Snow Buoys drifted with the sea ice for

120   two years or more, resulting in a correspondingly aged snow regime. For example, Snow Buoy 2014S10 remained adrift for almost three years, leading to measured snow depths pertaining to the 2-to-4-year snow regime.

2.3 One-dimensional thermodynamic sea ice model

    A simple one-dimensional thermodynamic ice growth model based on the number of freezing degree days (Thorndike, 1992), as used in Arndt et al. (2021), is applied to estimate the evolution of the thermodynamic sea ice growth at the bottom of the

125   ice and the resulting ice freeboard. For the latter, a simplified assumption is made that a calculated negative freeboard causes potential flooding of the snow/ice interface and subsequent snow-to-ice conversion, i.e., snow ice formation, both taking place in the same time step. Previous studies by Wever et al. (2021) have demonstrated that such an assumption tends to overestimate actual flooding and snow ice formation on a floe-scale, primarily due to the significant spatial heterogeneity of snow and ice thickness. To address and assess this limitation, the results of the model runs are evaluated alongside in-situ observations (refer

130   to section 2.5).

    Model runs are initialized with the measured initial sea ice thickness during buoy deployment. The atmospheric forcing of the model, i.e., surface temperature and heat fluxes, is based on ERA5 reanalysis data (Copernicus Climate Change Service, 2017), which were extracted for the nearest-neighbor grid points of the daily buoy positions.

    Reported values for ocean heat fluxes in the Weddell Sea vary, ranging from 2-7 Wm^2 (Lytle and Ackley, 1996; Robertson et

135   al., 1995) in the western part to well above 20 Wm^2 (McPhee et al., 1999) in the central part. Considering that the buoys primarily drift in the inner pack ice, the ocean heat flux for the simulations in this study is set toward the lower end of the range, prescribed with a constant flux of 3 Wm^2.

    For snow density and thermal conductivity regionally adjusted parameters, following Arndt (2022), are utilized. Specifically, snow densities of 340 kg m^{-3} and 264 kg m^{-3}, along with snow thermal conductivities of 0.28 $Wm^{-1}K^{-1}$ and 0.17 $Wm^{-1}K^{-1}$ for

140   perennial and seasonal sea ice, respectively, are applied. Further details regarding the model setup can be accessed in the appendix of Arndt et al. (2021).

2.4 Multi-layer snow model SNOWPACK

To estimate the amount of both snow ice and superimposed ice formed during the buoys' lifetime, we use the multi-layer snow cover model SNOWPACK. In the one-dimensional SNOWPACK model, snow microstructure is represented in detail and liquid water flow and refreezing processes are taken into account (Bartelt and Lehning, 2002; Lehning et al., 2002a; Lehning et al., 2002b; Wever et al., 2015; Wever et al., 2016). SNOWPACK was originally developed to represent physical processes in the snow cover in alpine regions, but has been adapted and applied to sea ice environments recently (Wever et al., 2021; Wever et al., 2020).

For our simulations, we initialize the model with the initial snow and ice thicknesses as measured during buoy deployment. The initial snow and ice temperature profile is determined from the ERA5 surface temperature and a water temperature of 271.35 K, assuming that the snow and ice column is in thermal equilibrium. For the remaining properties, we follow the approach of Wever et al. (2021): For the snow layers, we assume an initial density of 275 kg m^{-3}, corresponding to a volumetric ice content of 0.3 m3 m^{-3} and a volumetric air content of 0.7 m3 m^{-3}, and set the grain radius to 0.15 mm, the bond radius to 0.09 mm and sphericity and dendricity to 0. However, once snow ice has formed in the model, the densities of the corresponding layers may change in the simulation but they will still be referenced as snow ice in the analysis. For the ice layers above sea level, we assume the volumetric ice and air content to be 0.95 m^3 m^{-3} and 0.05 m^3 m^{-3}, respectively. Ice layers below sea level are assumed to contain also a fraction of water, calculated from the layers' temperature and an assumed bulk salinity of 1.75 g kg^{-1}.

Following the approach of Wever et al. (2021), we use the Richards equation, combined with the transport equation for salinity to solve liquid water and brine distributions. For two out of the 36 Snow Buoys (2017S49 and 2019S88) the simulations are aborted due to numerical instability and we use a more simple bucket-type approach instead of the Richards equation. In contrast to Wever et al. (2021), we choose an atmospheric stability following Holtslag and De Bruin (1988), as in the SNOWPACK model documentation this was changed to be the new default setting (the effect on the snow depth is minor). Like in the simple thermodynamic sea ice model described above, the ocean heat flux is set to a constant value of 3 Wm^{-2} and the atmospheric forcing is based on ERA5 reanalysis data, specifically surface heat fluxes, humidity, and surface wind.

Here, we present snow-height-driven simulations, which means that the SNOWPACK simulations are forced to closely follow the snow height evolution as measured by the Snow Buoy. While snow accumulation as indicated in the Snow Buoy datasets will lead to an instant increase in the SNOWPACK simulation (like a precipitation event), sudden reductions in snow height will only be incorporated within the scope of the model physics. Wind-induced transport of snow is neglected. The simulated snow densities are used to distinguish between snow (density $\leq$ 600 kg m^{-3}), superimposed ice (600 kg m^{-3} < density < 918 kg m^{-3}) and snow ice (density $\geq$ 918 kg m^{-3}).

2.5 In-situ data of snow and ice properties

To provide a comprehensive context for the Snow Buoy measurements and to validate the results of the one-dimensional thermodynamic sea ice model (Section 2.3), additional ice station work conducted during expeditions to the Weddell Sea in the late austral summer, i.e., February and March, is presented (Figure 1A). The ice station work during expedition PS124 of the German icebreaker *RV Polarstern* in 2021 focused on the southeastern Weddell Sea (Haas et al., 2021). In contrast, the ice stations of expedition PS118 (Haas et al., 2019), also conducted by *RV Polarstern*, and the expedition Endurance22, carried out with the South African icebreaker *S.A. Agulhas II* (Rabenstein, 2022), covered the northwestern Weddell Sea.

During these expeditions, snow depth was measured using a GPS-equipped Magna Probe (Snow Hydro, Sturm and Holmgren (2018)) along transect lines spanning several kilometers across the entire sampled ice floes. Additional analyses of ice cores, focusing on salinity and stable water isotopes, were performed to determine the fractions of superimposed ice and snow ice (e.g., Arndt et al., 2021).

3 Results and Discussion

3.1 Drift regimes in the Weddell Sea

As described in Section 2.1, a significant proportion of the sea ice in the Weddell Sea forms in the polynyas along the east coast and is subsequently transported north(-west) wards by the Weddell Gyre. In addition, the seasonal fast ice near Atka Bay drifts along its eastern coast into the Weddell Sea (e.g., Snow Buoy 2018S56). However, closer examination of the ice drift patterns reveals variations in the drift regimes (Figure 1A) (Schwegmann et al., 2011). Some of the sea ice floes formed in the southeastern Weddell Sea follow a rather pronounced northward trajectory, ending up in the marginal ice zone of the central and eastern Weddell Sea (e.g., 2016S37, Figure 1A). Other ice floes formed in the southeastern Weddell Sea drift on a longer southerly course, eventually ending up in the northwestern Weddell Sea (e.g., 2021S114, Figure 1A). However, the exact location of their origin along the eastern Weddell Sea coast and their subsequent drift trajectories do not have a clear geographical assignment. Instead, these trajectories are more influenced by geostrophic winds (Kottmeier et al., 1992), local sea ice/ocean/shelf ice interactions causing currents (Kottmeier and Sellmann, 1996), tides (Robertson et al., 1998), as well as the sea ice thickness and concentration (Vihma et al., 1996).

In addition, polynyas in the southern Weddell Sea, including the Ronne Polynya, also produce persistent sea ice (Haas et al., 2008). This ice is frequently transported westward by the Weddell Gyre, which then carries it north along the Antarctic Peninsula towards the northwestern Weddell Sea (e.g., 2018S59).

Considering the literature cited and the diverse drift trajectories observed for the Snow Buoys (Figure 1A), it is reasonable to assume that these buoys capture the prevailing drift patterns in the Weddell Sea. Therefore, the snow analyses conducted along the buoys' drift trajectories, as presented below, can be regarded as representative for the region as a whole.

3.2 Spatial and seasonal variability of snow accumulation rates
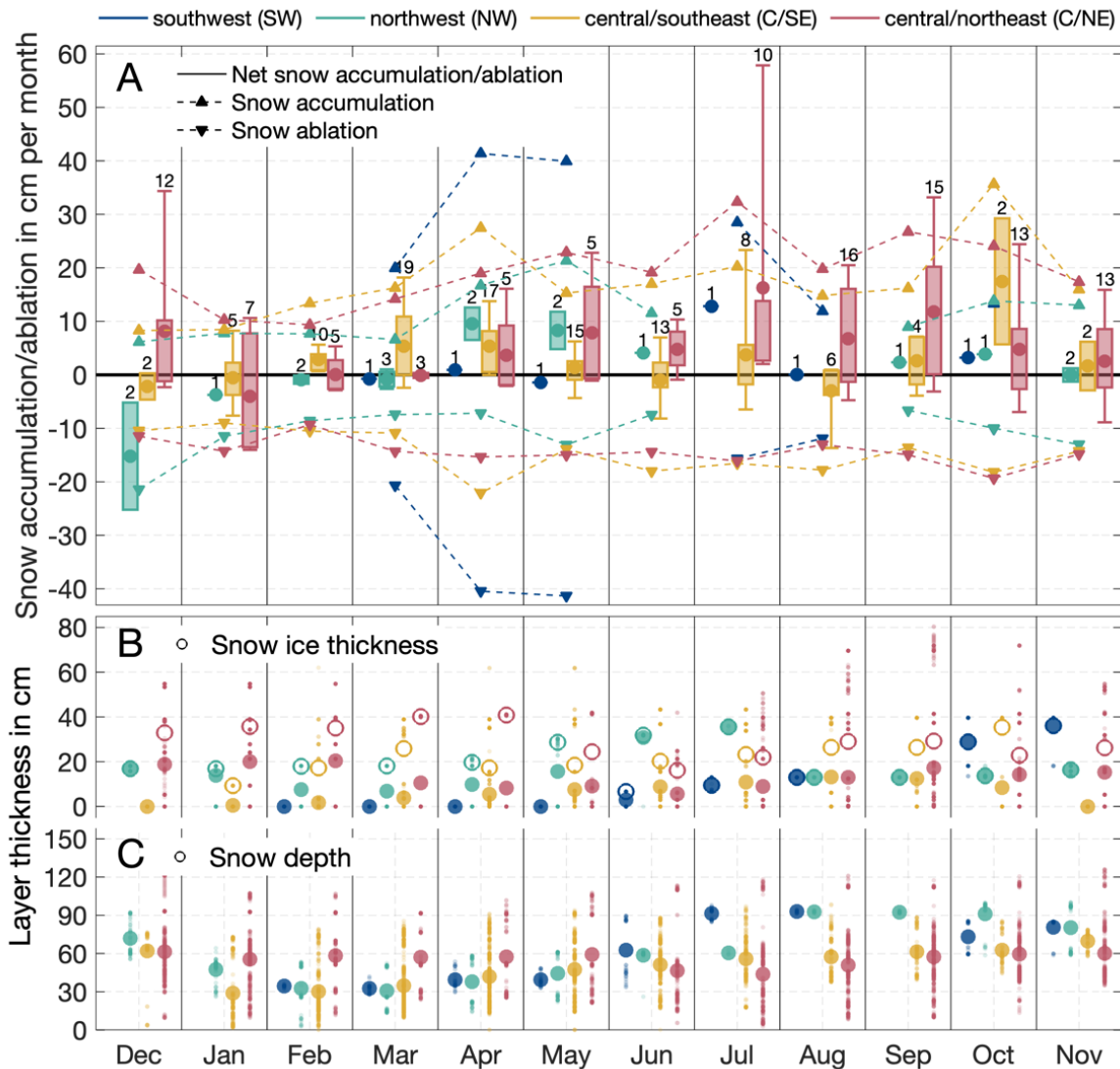
Figure 2. A Monthly mean snow accumulation rates (upward triangles), snow ablation (downward triangle), and net accumulation (positive) or ablation (negative) rates (boxplots) of all Snow Buoys separated for the four regions in the Weddell Sea (see Figure 1). Data were included if at least 25 days per cycle were available in the respective month and region. Numbers indicate the amount of annual buoy cycles contributing to the mean value. In the boxplots, boxes span over the first and third quartiles. The whiskers display the 10th and 90th percentiles; the circles indicate mean values, which may include contributions from both accumulation and ablation. Panels **B** and **C** display the calculated layer thicknesses of snow ice and snow, respectively, from the applied 1-D thermodynamic sea ice growth model. Small dots represent individual point calculations

for the specific month and region, while the large filled circles represent monthly regional means. Considering the transparency of the individual small dots, the higher the transparency, the fewer points are overlayed here, whereas the lower the transparency, the more points are overlayed. For snow ice, mean values are calculated by taking the overall mean (filled), as well as the pure mean snow ice thickness, i.e., averaging only over the cases where snow ice is actually present (open circles).

215

The Snow Buoy results underline that sea ice in the Weddell Sea is characterized by a year-round snow cover, highlighting the dynamic nature of snow processes. The Weddell Sea region shows remarkable differences in annual net accumulation/ablation patterns. In the central/northeastern (C/NE) Weddell Sea, an average net accumulation of 57 cm is observed, whereas in the northwestern (NW) Weddell Sea a significantly lower accumulation of only 8 cm is observed (Figure 1B and 2A). However,

220 when considering the annual mean of the actual snow accumulation rate, which includes potential snow-to-ice conversion, the mean values range from 52 ± 31 cm/year in the southeastern (C/SE) region to 66 ± 41 cm and 68 ± 33 cm in the C/NE and NW regions, respectively, and increase further to 74 ± 41 cm in the southwestern (SW) region (Figure 1B).

Examining individual time series of snow accumulation recorded by the Snow Buoys (Figure 3B/D) reveals that snow accumulation takes place throughout the year driven by both continuous deposition and occasional events. Overall, the seasonal

225 cycle of net snow accumulation/ablation is generally modest for most regions (Figure 2A), which is in agreement with the seasonal cycle of precipitation derived from reanalysis data in the region (e.g., Boisvert et al., 2020). However, the SW region is dominated by perennial sea ice, and the associated limitations on buoy deployments, and thus data availability hinders a comprehensive seasonal analysis (Figure 1A).

For the C/NE Weddell Sea, the period from May to December shows the largest monthly net snow accumulation (Figure 2A),

230 which can be attributed to its closer proximity to the ice edge, along with typical eastward-moving cyclone paths, causing precipitation in the region (Boisvert et al., 2020). Also, the C/SE Weddell Sea experiences above average net snow accumulation in October, which may be due to local topographic effects associated with, for example, the grounded iceberg A23A. The iceberg acts as a barrier, blocking the westward movement of sea ice in the area, and thus influences snow accumulation patterns towards significantly higher accumulation rates, as observed for Snow Buoys 2014S10 and 2014S12

235 (Nicolaus et al., 2021).

In contrast, significant snow depth reduction or melt is mainly observed during the summer months in the Marginal Ice Zone (MIZ), with monthly net snow mass loss/melt occurring exclusively in December and January (Figure 2A). Here, a maximum snow loss of 15 cm / month is observed in the NW Weddell Sea in December, while the C/NE Weddell Sea experiences a loss of 4 cm in January. The C/SE region, however, exhibits a relatively low ablation period compared to other regions between

240 May and August, with an average loss of up to 3 cm / month. This phenomenon could be linked to snow compaction and redistribution caused by katabatic winds originating from the east coast of the Weddell Sea (Venegas and Drinkwater, 2001).

The observed latitudinal patterns of snow mass loss in the Weddell Sea region are consistent with satellite radiometric analyses of seasonal snowmelt processes, indicating a consistent latitudinal gradient in the timing and intensity of snowmelt (Arndt et al., 2016; Willmes et al., 2009).

245 Based on the data from the 36 Snow Buoys, the Weddell Sea shows spatial and temporal variability in snow accumulation and ablation, with particularly high accumulation rates in the predominantly perennial sea ice areas of the southern and western regions. Therefore, considering the hydrostatic equilibrium of sea ice, the question arises as to how much of the initially accumulated snow remains as snow until the end of the ice floe or buoy drift, and how much has been transformed into meteoric ice over time, which is addressed in the following section.

250 **3.3 Seasonal transition of snow into snow ice**

Considering the often-high snow accumulation rates presented in Section 3.2 and the hydrostatic equilibrium of sea ice, it becomes clear that not all of the snow that has fallen on sea ice remains snow. Instead, the snow is transformed into snow ice at the snow-ice interface. Thus, the snow accumulation does not equal snow depth, but has to be corrected for the snow ice fraction. To achieve this, a one-dimensional thermodynamic sea ice model is applied along the drift trajectories of each Snow

255 Buoy, yielding both the thermodynamic sea ice growth or melt at the bottom and the snow ice formation at the top (Figure 3B and 4). The model is forced with the sea ice thickness at the time of buoy deployments, the daily-averaged snow accumulation retrieved from the Snow Buoys, and the surface heat fluxes obtained from the ERA5 reanalysis data. For the subsequent analysis, it is important to note that the snow ice thickness may be overestimated, as negative freeboards are directly translated into flooding and subsequent snow ice formation, which may not always be the case (see, e.g., Wever et al. (2021)).

260 The results show that the model detects potential snow ice formation along 41% of the total track length of the analyzed Snow Buoy tracks, with the snow ice layer observed in 16 of the analyzed buoys (Figure 1C). This was particularly the case for buoys deployed on the fast ice at the northeastern edge of the Weddell Sea, which then drifted with the Weddell Gyre, and for buoys in the western Weddell Sea, i.e., in the perennial ice regime. The mean maximum thickness of snow ice for these 16 ice floes was 35 cm, which accounts for 27% of the snow accumulation. Taking the whole data set, including ice floes without

265 snow ice, the mean maximum snow ice thickness is 16 cm for the Weddell Sea (Figure 2B).

3.3.1 Eastern Weddell Sea
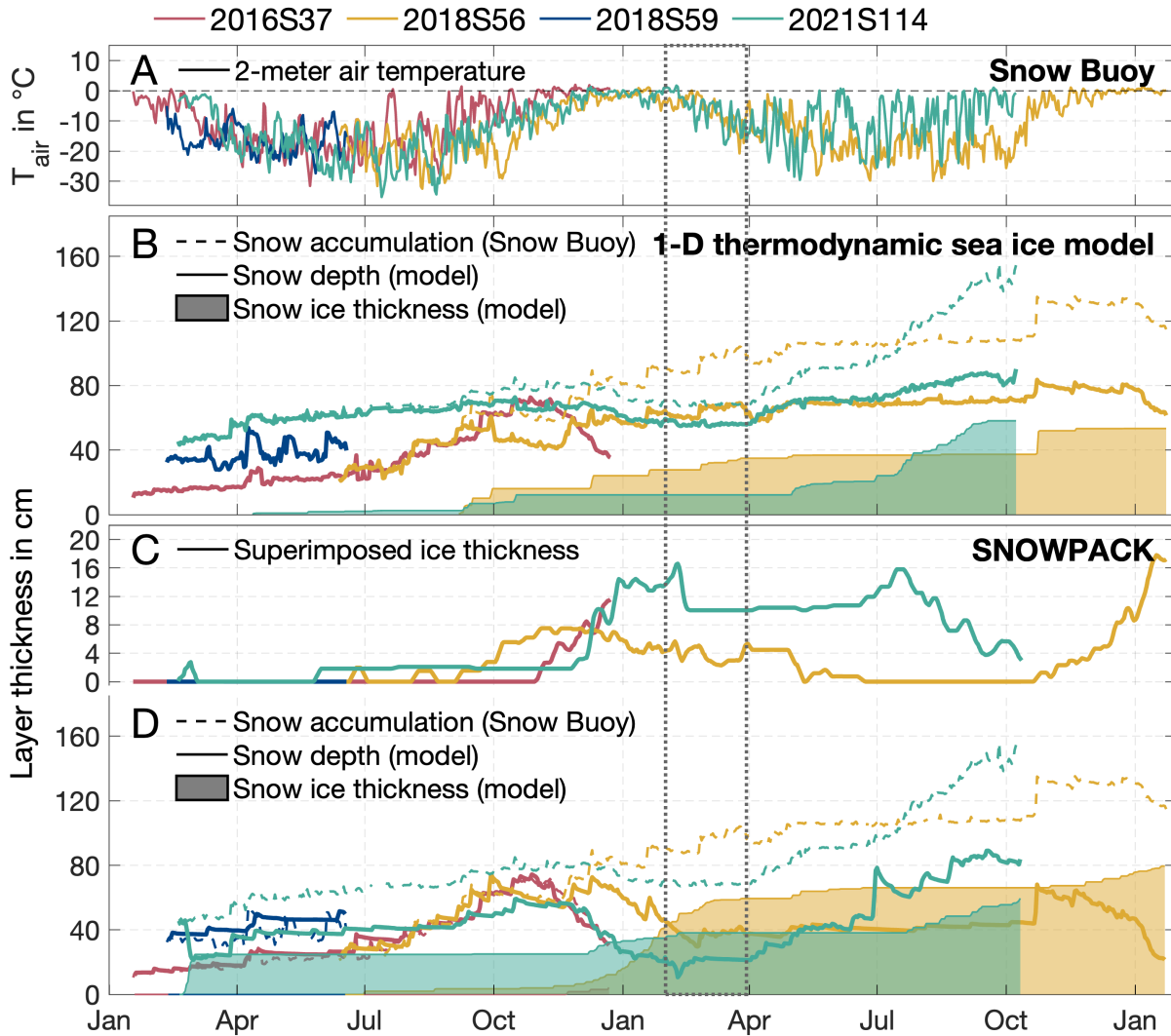
Figure 3. Time series of **A** 2-meter air temperature measured by the presented Snow Buoys and results from **B** the applied 1-D thermodynamic sea ice growth model and **D** the snow model SNOWPACK for layer thicknesses of the snow accumulation retrieved from the Snow Buoys (dashed lines) and the calculated snow depth (solid lines) and snow ice thickness (filled areas), and additional superimposed ice layer thickness in **C**. The colors represent the four exemplary Snow Buoys 2016S37 (red), 2018S56 (yellow), 2018S59 (blue) and 2021S114 (green) (Figure 1). The data are plotted for the corresponding months, with the buoy deployment year indicated by the buoy name (e.g., buoy 2016S37 is deployed in 2016). The dashed box across all panels indicates the time frame of the corresponding field data (Figure 1).

In the C/SE region, the maximum monthly mean snow ice thickness is reached in late spring, i.e., October, with an average of 35 ± 10 cm. This value coincides well with the time of maximum snow accumulation in the region, as shown in Figure 2A. Furthermore, the calculated snow ice thickness in February/March was found to be 23 ± 15 cm, which is reasonably consistent with the observed snow ice thickness of 21 ± 18 cm, ranging from 0 to 58 cm, obtained from ice cores taken on 19 different ice floes in the same region in 2021 (Figure 1A, Arndt (2022)). However, while only 14% of the Snow Buoy data points indicate potential snow ice formation in February/March (Figure 2B), 84% of the analyzed ice cores in the southeastern Weddell Sea (16 out of 19) confirm the presence of snow ice (Arndt, 2022).

Correcting the snow accumulation for the calculated snow ice thickness reveals an even weaker seasonal cycle in snow depth compared to the snow accumulation rates discussed before (Section 2.2), especially in the C/NE Weddell Sea. Here, the highest monthly mean snow depth of 62 cm is observed in December and the lowest monthly mean snow depth of 45 cm in July (Figure 2C). In contrast, the C/SE Weddell Sea shows the highest snow depth in November and the lowest in February, with mean values of 70 cm and 30 cm, respectively (Figure 2C). For the months of February/March, the corrected mean snow depth values of 33 ± 22 cm agree well with the measured snow depths of 35 ± 23 cm on average during the *RV Polarstern* expedition PS124 in 2021. The C/SE Weddell Sea is not significantly impacted by additional internal processes such as superimposed ice formation (Arndt, 2022; Nicolaus et al., 2009), due to the high southern latitudes, the proximity to the continent, and associated cold katabatic winds (Ebner et al., 2014). Therefore, it can be concluded that the retrieved snow depth values for the C/SE Weddell Sea presented here correspond to the actual values and that the model parameters used appear to be representative for this region.

3.3.2 Western Weddell Sea

For the SW Weddell Sea, the highest snow ice layer thicknesses are obtained in October and November with 29 ± 11 and 36 ± 8 cm, respectively (Figure 2C). For the NW Weddell Sea, the maximum monthly mean snow ice thickness is observed in July with 35 cm.

However, these monthly mean values for the region are not statistically significant as they are based on only 29 and 24 (SW) and 4 data points (NW) from a single buoy, respectively (Figure 2C). Nevertheless, the data are important to demonstrate the potential for the thickest snow ice layers to occur in the western Weddell Sea, i.e., that most snow is converted to snow ice in the predominantly perennial sea ice regime. This is also supported by observations made in February/March 2022 in the region during the Endurance22 expedition (Rabenstein, 2022). Using ice core data, from which snow, meteoric ice and thermodynamically grown ice can be distinguished by salinity and stable water isotope analyses, snow ice thicknesses between 2 and 89 cm were determined, with a mean value of 38 ± 24 cm, which aligns well the modelled snow ice thicknesses.

However, when considering the snow ice thicknesses calculated along the trajectory of Snow Buoy 2021S114 in February/March 2022 (Figure 1C), which was approximately 100 km away from the ice stations of the concurrent Endurance22

expeditions, the sea ice model gives a mean snow ice thickness of only 12 cm (Figure 3B), i.e., one third of the measured layer thickness during the Endurance22 expedition, as mentioned above. This discrepancy can be attributed to two possible causes: First, Nicolaus et al. (2021) showed that snow accumulation rates can vary considerably on spatial scales smaller than 250 km. This variation in snow accumulation rates can be reassessed for the Endurance22 expedition by using the measured snow and

310   snow ice thicknesses, under the assumption of a one-to-three ratio between snow and snow ice densities. Accordingly, an estimated snow accumulation of approximately 120 cm is derived for the sampled ice floes during the Endurance22 expedition, while the Snow Buoy 2021S114 had accumulated only approximately 70 cm of snow until February 2022. These variations in snow accumulation may be due to the Snow Buoys usually being deployed on level ice and therefore do not account for snow drifting and accumulating in ice ridges. Thus, the Snow Buoy data may have a bias towards underestimating snow

315   accumulation, and consequently also underestimating snow ice formation. Second, the thermodynamic sea ice model used here assumes a constant ocean heat flux. During spring/summer 2022, the sea ice edge was further south than usual (e.g., Turner et al., 2022), raising the possibility of a higher ocean heat flux, resulting in more bottom sea ice melting and subsequently more potential for flooding and snow ice formation. This assumption is supported by observational data on sea ice thickness in the Weddell Sea. During the Endurance22 expedition in February 2022, conducted in the northwestern Weddell Sea, a

320   predominant sea ice thickness of 1.05 meters was recorded (Rabenstein, 2022). Contrarily, data from the previous summer in the southeastern Weddell Sea, in February/March 2021, indicated a modal sea ice thickness of 1.5 meters (Arndt, 2022), highlighting the associated significant bottom melt, and related flooding and snow ice formation processes in the region. Thus, doubling the ocean heat flux from 3 to 6 Wm^{-2}, the modelled snow ice thickness for the ice floe of Snow Buoy 2021S114 increases by 6 cm, highlighting the high sensitivity of the calculations to the ocean heat flux, especially in the marginal ice

325   zone. However, for the inner ice pack, the highly heterogeneous patterns of snow accumulation appear to be the major contributor to the variability in snow ice formation, as shown above.

This discrepancy continues in the actual snow depths calculated: while the model calculates a mean snow depth in the NW Weddell Sea of 35 ± 19 cm and 33 ± 18 cm for February and March (Figure 2D), respectively, the field measurements reveal a snow depth of 15 ± 11 cm (Rabenstein, 2022). It is important to highlight that the ice floes and Snow Buoys present in the

330   region are at least three, and in some cases, even four years old. As a result, the measured snow depths represent the corresponding perennial snow layers, a common occurrence in the region (Melsheimer et al., 2023). This is evident from the calculated maximum snow depths of 81 and 93 cm observed between August and November in the western Weddell Sea (Figure 2D). Therefore, in order to compile a complete snow climatology for the region, the snow depth values presented here must be assigned to corresponding ice age classes, which is beyond the scope of this study.

335   The calculated snow depths presented here correct the snow accumulation only for snow ice formation but do not consider other snow-to-ice conversion processes, such as superimposed ice formation, or sublimation. These additional processes decrease snow depth even more in this relatively northern region with elevated surface energy fluxes (Nicolaus et al., 2006; Arndt et al., 2021), and will be discussed in detail in the following Section 3.4.

3.4 Quantitative impact of snow metamorphism on the actual snow depth

340   The one-dimensional thermodynamic sea ice model used allows the description of the snow-to-ice conversion process by adjusting the snow-ice interface, maintaining the hydrostatic equilibrium of the sea ice and its snow cover. However, air temperature measurements from the analyzed Snow Buoys show temporary occurrences of temperatures around the freezing point (Figure 3A), especially during the summer season. This suggests the possibility of internal snow melting followed by refreezing, leading to the formation of superimposed ice. In order to quantitatively assess the contribution of superimposed

345   ice, the snow model SNOWPACK was used in a simplified configuration, excluding wind-driven snow drift processes. However, it is imperative to account for uncertainties, notably the differentiation between snow ice and superimposed ice, which relies solely on density values (as discussed in Section 2.4).

    In this context, 58% of the analyzed buoy data points have superimposed ice thickness calculated, which is characterized by an average maximum layer thickness of 7 ± 5 cm per buoy track (Figure 4A). However, the analysis excludes Snow Buoy

350   2014S12 due to its maximum superimposed ice thickness of 29 cm, which is an outlier caused by an extended period spent at high northern latitudes (Nicolaus et al., 2021). Also Snow Buoys 2018S56 and 2021S114 spent a considerable amount of time in the northern latitudes causing a maximum superimposed ice thickness of 19 and 20 cm. For all other buoys, the thickness of the maximum superimposed ice layer ranges between 0 and 16 cm, with a tendency towards thicker layers at more northern latitudes and thinner layers or no superimposed ice south of 70°S (Figure 4A).

355   The findings presented here agree with superimposed ice observations during recent expeditions to the Weddell Sea: Though the ice core analysis from PS124 expedition conducted in March 2021 did not detect any superimposed ice in the southeastern Weddell Sea, the same ice regime that moved into the northwestern Weddell Sea in March 2022 showed an average superimposed ice thickness of 8 ± 5 cm, varying from 0 to 17 cm (Haas et al., 2021; Rabenstein, 2022). Also the ice regime in the northwestern Weddell Sea originating from the southwest shows a mean superimposed ice thickness of 11 ± 11 cm at the

360   end of summer 2019 (Arndt et al., 2021). Both, observations and snow model results, indicate that the thickness of the superimposed ice layer displays a latitude-dependent gradient. This is in agreement with the internal snowmelt onset calculated using passive and active microwave satellite data. The results show that the detection of seasonal internal melt-freeze cycles occurs earlier at more northern locations: the more northern the location, the earlier the detection of seasonal internal melt-freeze cycles (Arndt and Haas, 2019; Arndt et al., 2016). These processes correlate with the latitude-dependent surface energy

365   fluxes.

    The latitude-dependent superimposed ice formation is also reflected in the comparison of snow depths between the one-dimensional sea ice model and the SNOWPACK model (Figure 4B), where the actual snow depth tends to be thinner because not only the snow ice but also the superimposed ice formation is taken into account. This is particularly the case for buoys 2018S56 and 2021S114 that have been drifting for a long time in more northern latitudes and have therefore experienced more

370   melting. These results demonstrate the potential of using snow models to reduce uncertainties in estimating snow depth from

snow accumulation data on Antarctic sea ice. However, processes such as snow redistribution by drift processes are not yet included – a requirement that, in combination with the snow-to-ice conversion processes discussed here, will play an important role in the development of future snow models on sea ice in order to be able to close the snow mass budget on Antarctic sea ice.
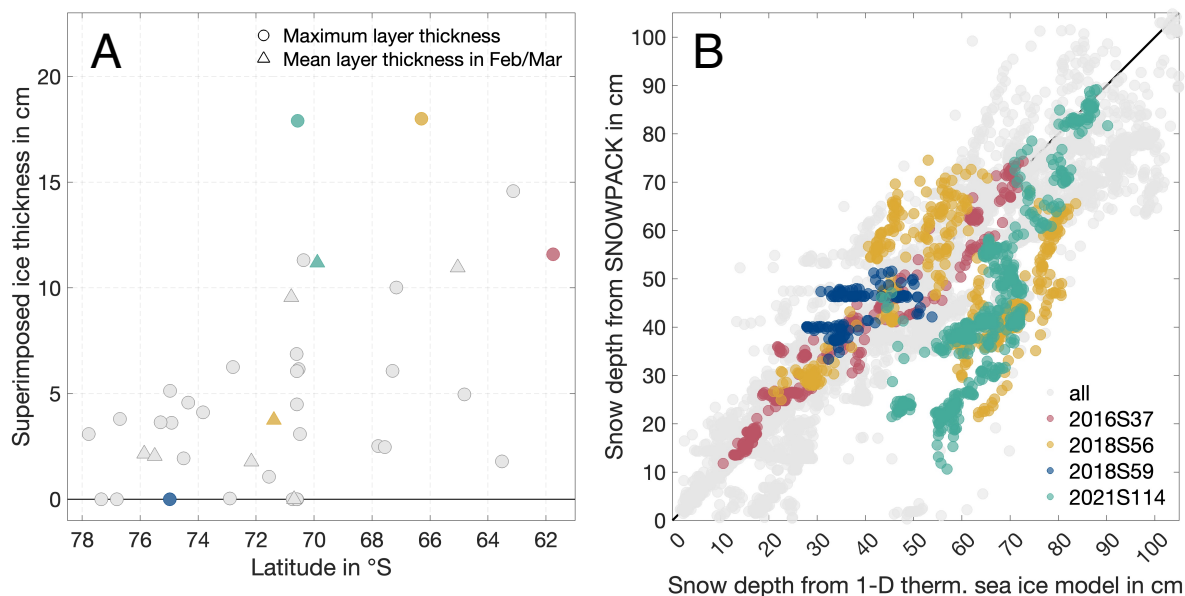
375

Figure 4. A Maximum layer thickness over the whole time series (circles) and mean layer thickness (triangles) over the February to March period of superimposed ice as a function of latitude. **B.** Correlation of snow depth estimates obtained by the one-dimensional sea ice model (x-axis) and SNOWPACK (y-axis). The diagonal line represents perfect agreement between the two models. Grey markers represent the respective calculations for all Snow Buoys, while colored markers represent the four exemplary Snow Buoys 2016S37 (red), 2018S56 (yellow), 2018S59 (blue) and 2021S114 (green) (Figure 1).

380

4 Summary and Conclusion

In this study, we used a comprehensive snow accumulation dataset acquired from Snow Buoys deployed on level ice drifting in the Weddell Sea over the last decade. Our primary objective was to derive the actual snow depth from snow accumulation and surface elevation data. This was achieved by assessing potential snow ice layer thicknesses along the drift trajectories using a one-dimensional thermodynamic sea ice model. In addition, we used the snow model SNOWPACK to account for key snow metamorphism processes, including the formation of superimposed ice.

385

Our results highlight that snow ice formation takes place primarily in the eastern Weddell Sea. In this region, the combination of sea ice growth at the snow/ice interface through snow-to-ice conversion processes and the insulating properties of snow act as a barrier to significant thermodynamic growth during the winter months. Thus, as it drifts towards the northwestern Weddell

390   Sea, the rather thick sea ice, from both thermodynamic and meteoric ice growth, limits the formation of additional snow ice during the winter season. However, the potential for snow ice formation returns in summer, driven by the onset of bottom melt and increased snowfall, particularly in response to the influx of warmer, moister air masses towards the ice edge. As a result, our analysis suggests that the thickest snow ice layers within the perennial sea ice zones of the northwestern Weddell Sea are primarily sourced from the southeastern Weddell Sea, owing to the sequential snow ice formation process occurring first in

395   the southeastern region and then extending to the northwestern Weddell Sea. This phenomenon is due to the balancing effects of hydrostatic equilibrium, which maintain a consistent snow layer thickness even in regions characterized by high snow accumulation rates, such as the southwestern Weddell Sea, or during localized instances of intense snowfall where large amounts of snow ice are formed.

   The evidence of current declining sea ice extent and concentration in the Southern Ocean suggests the possibility of increased

400   ocean heat fluxes in the coming years and decades (e.g., Eayrs et al., 2021; Purich and Doddridge, 2023). These changes could lead to increased rates of bottom sea ice melt, increasing the likelihood of flooding and associated snow ice formation. At the same time, warmer air temperatures are expected to allow for higher moisture content, leading to increased snowfall and hence increased potential for flooding and snow ice formation. Concurrently, however, warming air temperatures and the associated shift in the surface energy fluxes above the sea ice may also increase snow mass loss through surface melting. This

405   metamorphic and wet snow reduces the albedo and eventually leads to an ice-albedo feedback-supported appearance of melt ponds caused by more Arctic-like atmospheric conditions, which is referred to as "Arctification" of the Antarctic sea ice (Arndt et al., 2021).

   We acknowledge that our assumption on ocean heat flux does not take into account its regional and temporal variability, potentially causing ocean heat flux and thus snow ice formation to be underestimated. Additionally, the immediate assumption

410   of snow ice formation with negative freeboard may result in an overestimation of actual flooding and snow ice formation. While these processes may balance each other out, future research could enhance process understanding at the snow/ice and ice/ocean interface, for instance, through the deployment of autonomous thermistor string buoys, aiming for improved evaluation of the presented results.

   In conclusion, this study underscores the critical importance of understanding snow transformation processes, not only under

415   current conditions, but also in anticipation of future changes in the coupled Antarctic sea ice system. These hidden processes, i.e., the formation of snow ice and superimposed ice, will remain hidden, while large-scale analyses will have increasing importance, based on model and satellite remote sensing data. It is imperative to further develop and refine existing snow models to better reflect Antarctic sea ice conditions. This will enable us to close the Antarctic snow mass budget and improve the estimates of Antarctic sea ice thickness derived from both sea ice modelling and satellite remote sensing applications. A

420   full understanding of these processes is essential to capture the complex dynamics of the Antarctic sea ice environment and its response to ongoing climate change.

Data availability

Snow accumulation measurements from Snow Buoys were obtained from https://www.meereisportal.de (grant: REKLIM-2013-04) and are stored in PANGAEA (Nicolaus et al., 2021, https://doi.pangaea.de/10.1594/PANGAEA.875638).

425 All ERA5 data from ECMWF are accessed and downloaded from the Copernicus Climate Change Service (last access: 29 September 2023): https://cds.climate.copernicus.eu/cdsapp#!/dataset/reanalysis-era5-single-levels?tab=form.

All snow depth data from ice station work are available at https://doi.org/10.1594/PANGAEA.946183 (Arndt, 2022), https://doi.pangaea.de/10.1594/PANGAEA.928966 (Arndt & Haas, 2021), and https://doi.pangaea.de/10.1594/PANGAEA.946177 (Arndt & Haas, 2022).

430 MeteoIO and SNOWPACK are software published under a GNU LGPLv3 license by the WSL Institute for Snow and Avalanche Research SLF at https://gitlabext.wsl.ch/snow-models. The model source code used in this study was downloaded on 26 April 2023.

Authors contribution

SA and MN coordinated the deployment of the Snow Buoys in the Weddell Sea. SA set up and performed the one-dimensional
435 thermodynamic sea ice model, while NM and LR set up and performed the SNOWPACK model runs. SA performed all analyses and prepared the figures for the paper. All authors contributed to discussions and the actual writing.

Competing interests

The authors declare that they have no conflict of interest.

Acknowledgements

440 We gratefully acknowledge the support of the cruise leaders, all involved scientists, the helicopter teams on board, and the captains and crews of *R/V Polarstern* during expeditions PS81, PS82, PS89, PS96, PS103, PS111, and PS124 (grant numbers AWI_PS81_00, AWI_PS82_02, AWIPS89_02, AWI_PS96_01, AWI_PS103_02, AWI_PS111_00, AWI_PS124_08). In the same way, we acknowledge the work of all people involved of the Endurance22 expedition with the *S.A. Agulhas II*. Furthermore, we acknowledge all wintering teams at Neumayer Station III supporting the regular deployment of buoys in Atka
445 Bay near the base. We highly appreciate the work of the www.meereisportal.de team for building and maintaining the online platform and database for all Snow Buoy data (REKLIM-2012-04).

Financial support

This work received funding from the German Research Foundation's (DFG) projects fAntasie (AR1236/3-1), SnowCast (AR1236/1-1), SCASI (NI1096/5-1) and SCASI-RS (MA 5056/2-1) within its priority program "Antarctic Research with comparative investigations in the Arctic ice areas" (SPP1158), the DFG Emmy Noether Programme project SNOWflAke (project number 493362232), the University of Hamburg, and the Alfred-Wegener-Institut, Helmholtz-Zentrum für Polar- und Meeresforschung. All buoys were funded by the Helmholtz infrastructure programmes ACROSS and FRAM with contributions for data transmission by the German Weather service (DWD) and the International Arctic Buoy Program (IABP).

References

Ackley, S., Lewis, M., Fritsen, C., and Xie, H.: Internal melting in Antarctic sea ice: Development of "gap layers", Geophysical Research Letters, 35, https://doi.org/10.1029/2008GL033644, 2008.

Ackley, S., Perovich, D., Maksym, T., Weissling, B., and Xie, H.: Surface flooding of Antarctic summer sea ice, Annals of Glaciology, 1-10, 10.1017/
aog.2020.22, 2020.

Arndt, S., Willmes, S., Dierking, W., and Nicolaus, M.: Timing and regional patterns of snowmelt on Antarctic sea ice from passive microwave satellite observations, Journal of Geophysical Research - Oceans, 121, 5916-5930, 10.1002/2015JC011504, 2016.

Arndt, S., and Haas, C.: Spatiotemporal variability and decadal trends of snowmelt processes on Antarctic sea ice observed by satellite scatterometers, The Cryosphere, 13, 1943-1958, 10.5194/tc-13-1943-2019, 2019.

Arndt, S., Hoppmann, M., Schmithüsen, H., Fraser, A. D., and Nicolaus, M.: Seasonal and interannual variability of landfast sea ice in Atka Bay, Weddell Sea, Antarctica, The Cryosphere, 14, 2775-2793, 10.5194/tc-14-2775-2020, 2020.

Arndt, S., Haas, C., Meyer, H., Peeken, I., and Krumpen, T.: Recent observations of superimposed ice and snow ice on sea ice in the northwestern Weddell Sea, The Cryosphere, 15, 4165-4178, 10.5194/tc-15-4165-2021, 2021.

Arndt, S.: Sensitivity of Sea Ice Growth to Snow Properties in Opposing Regions of the Weddell Sea in Late Summer, Geophysical Research Letters, 49, e2022GL099653, https://doi.org/10.1029/2022GL099653, 2022.

Bartelt, P., and Lehning, M.: A physical SNOWPACK model for the Swiss avalanche warning: Part I: numerical model, Cold Regions Science and Technology, 35, 123-145, 2002.

Boisvert, L. N., Webster, M. A., Petty, A. A., Markus, T., Cullather, R. I., and Bromwich, D. H.: Intercomparison of precipitation estimates over the Southern Ocean from atmospheric reanalyses, Journal of Climate, 33, 10627-10651, 2020.

Calonne, N., Flin, F., Morin, S., Lesaffre, B., du Roscoat, S. R., and Geindreau, C.: Numerical and experimental investigations of the effective thermal conductivity of snow, Geophysical Research Letters, 38, 10.1029/2011gl049234, 2011.

Copernicus Climate Change Service: ERA5: Fifth generation of ECMWF atmospheric reanalyses of the global climate, https://cds.climate.copernicus.eu/cdsapp#!/home, 2017.

Eayrs, C., Li, X., Raphael, M. N., and Holland, D. M.: Rapid decline in Antarctic sea ice in recent years hints at future change, Nature Geoscience, 14, 460-464, 10.1038/s41561-021-00768-3, 2021.

Ebner, L., Heinemann, G., Haid, V., and Timmermann, R.: Katabatic winds and polynya dynamics at Coats Land, Antarctica, Antarct Sci, 26, 309-326, 2014.

Eicken, H., Lange, M. A., Hubberten, H. W., and Wadhams, P.: Characteristics and distribution patterns of snow and meteoric ice in the Weddell Sea and their contribution to the mass balance of sea ice, Annales Geophysicae-Atmospheres Hydrospheres and Space Sciences, 12, 80-93, 10.1007/s00585-994-0080-x, 1994.

Fons, S. W., and Kurtz, N. T.: Retrieval of snow freeboard of Antarctic sea ice using waveform fitting of CryoSat-2 returns, The Cryosphere, 13, 861-878, 2019.

Grosfeld, K., Treffeisen, R., Asseng, J., Bartsch, A., Bräuer, B., Fritzsch, B., Gerdes, R., Hendricks, S., Hiller, W., and Heygster, G.: Online sea-ice knowledge and data platform < www. meereisportal. de >, Polarforschung, 85, 143-155, 2015.

Haas, C., and Eicken, H.: Interannual variability of summer sea ice thickness in the Siberian and central Arctic under different atmospheric circulation regimes, Journal of Geophysical Research: Oceans, 106, 4449-4462, 2001.

Haas, C., Thomas, D. N., and Bareiss, J.: Surface properties and processes of perennial Antarctic sea ice in summer, Journal of Glaciology, 47, 613-625, 10.3189/172756501781831864, 2001.

Haas, C., Nicolaus, M., Willmes, S., Worby, A., and Flinspach, D.: Sea ice and snow thickness and physical properties of an ice floe in the western Weddell Sea and their changes during spring warming, Deep-Sea Res Pt Ii, 55, 963-974, 10.1016/J.Dsr2.2007.12.020, 2008.

Haas, C., Arndt, S., Peeken, I., and Allhusen, E.: Chapter Sea Ice in: The Expedition PS118 of the Research Vessel POLARSTERN to the Weddell Sea in 2019, Berichte zur Polar-und Meeresforschung= Reports on polar and marine research, 735, 97-123, 10.2312/BzPM_0735_2019, 2019.

Haas, C., Arndt, S., Peeken, I., Eggers, S. L., and Neudert, M.: Chapter Sea Ice Geophysics and Biogeochemistry in: The Expedition PS124 of the Research Vessel POLARSTERN to the Weddell Sea in 2021, Berichte zur Polar-und Meeresforschung= Reports on polar and marine research, 2021.

Harms, S., Fahrbach, E., and Strass, V. H.: Sea ice transports in the Weddell Sea, Journal of Geophysical Research: Oceans, 106, 9057-9073, https://doi.org/10.1029/1999JC000027, 2001.

Kawamura, T., Ohshima, K., Takizawa, T., and Ushio, S.: Physical, structural, and isotopic characteristics and growth processes of fast sea ice in Lützow-Holm Bay, Antarctica, Journal of Geophysical Research: Oceans, 102, 3345-3355, 1997.

Kottmeier, C., Olf, J., Frieden, W., and Roth, R.: Wind forcing and ice motion in the Weddell Sea region, Journal of Geophysical Research: Atmospheres, 97, 20373-20383, 1992.

Kottmeier, C., and Sellmann, L.: Atmospheric and oceanic forcing of Weddell Sea ice motion, Journal of Geophysical Research: Oceans, 101, 20809-20824, 1996.

Kwok, R., and Kacimi, S.: Three years of sea ice freeboard, snow depth, and ice thickness of the Weddell Sea from Operation IceBridge and CryoSat-2, The Cryosphere, 12, 2789-2801, 2018.

Kwok, R., Kacimi, S., Webster, M., Kurtz, N., and Petty, A.: Arctic snow depth and sea ice thickness from ICESat-2 and CryoSat-2 freeboards: A first examination, Journal of Geophysical Research: Oceans, 125, e2019JC016008, 2020.

515 Lehning, M., Bartelt, P., Brown, B., and Fierz, C.: A physical SNOWPACK model for the Swiss avalanche warning Part III: meteorological forcing, thin layer formation and evaluation, Cold Regions Science and Technology, 35, 169-184, 2002a.

Lehning, M., Bartelt, P., Brown, B., Fierz, C., and Satyawali, P.: A physical SNOWPACK model for the Swiss avalanche warning: Part II. Snow microstructure, Cold regions science and technology, 35, 147-167, 2002b.

Lytle, V., and Ackley, S.: Heat flux through sea ice in the western Weddell Sea: Convective and conductive transfer processes, 520 Journal of Geophysical Research: Oceans, 101, 8853-8868, 1996.

Massom, R., Eicken, H., Haas, C., Jeffries, M. O., Drinkwater, M. R., Sturm, M., Worby, A. P., Wu, X. R., Lytle, V. I., Ushio, S., Morris, K., Reid, P. A., Warren, S. G., and Allison, I.: Snow on Antarctic Sea ice, Rev Geophys, 39, 413-445, 10.1029/2000rg000085, 2001.

McPhee, M. G., Kottmeier, C., and Morison, J. H.: Ocean heat flux in the central Weddell Sea during winter, Journal of 525 Physical Oceanography, 29, 1166-1179, 1999.

Melsheimer, C., Spreen, G., Ye, Y., and Shokr, M.: First results of Antarctic sea ice type retrieval from active and passive microwave remote sensing data, The Cryosphere, 17, 105-126, 10.5194/tc-17-105-2023, 2023.

Nicolaus, M., Haas, C., Bareiss, J., and Willmes, S.: A model study of differences of snow thinning on Arctic and Antarctic first-year sea ice during spring and summer, Annals of Glaciology, 44, 147-153, 10.3189/172756406781811312, 2006.

530 Nicolaus, M., Haas, C., and Willmes, S.: Evolution of first-year and second-year snow properties on sea ice in the Weddell Sea during spring-summer transition, Journal of Geophysical Research, 114, 10.1029/2008JD011227, 2009.

Nicolaus, M., Hoppmann, M., Arndt, S., Hendricks, S., Katlein, C., Nicolaus, A., Rossmann, L., Schiller, M., and Schwegmann, S.: Snow Depth and Air Temperature Seasonality on Sea Ice Derived From Snow Buoy Measurements, Frontiers in Marine Science, 8, 10.3389/fmars.2021.655446, 2021.

535 Paul, S., Willmes, S., and Heinemann, G.: Long-term coastal-polynya dynamics in the southern Weddell Sea from MODIS thermal-infrared imagery, The Cryosphere, 9, 2027-2041, 10.5194/tc-9-2027-2015, 2015.

Paul, S., Hendricks, S., Ricker, R., Kern, S., and Rinne, E.: Empirical parametrization of Envisat freeboard retrieval of Arctic and Antarctic sea ice based on CryoSat-2: progress in the ESA Climate Change Initiative, The Cryosphere, 12, 2437-2460, 10.5194/tc-12-2437-2018, 2018.

540 Purich, A., and Doddridge, E. W.: Record low Antarctic sea ice coverage indicates a new sea ice state, Communications Earth & Environment, 4, 314, 10.1038/s43247-023-00961-9, 2023.

Rabenstein, L.: Endurance22, Cruise Scientific Report, 1–95, 2022.

Ricker, R., Hendricks, S., Perovich, D. K., Helm, V., and Gerdes, R.: Impact of snow accumulation on CryoSat-2 range retrievals over Arctic sea ice: An observational approach with buoy data, Geophysical Research Letters, 42, 4447-4455, 2015.

545 Robertson, R., Padman, L., and Levine, M. D.: Fine structure, microstructure, and vertical mixing processes in the upper ocean in the western Weddell Sea, Journal of Geophysical Research: Oceans, 100, 18517-18535, 1995.

Robertson, R., Padman, L., and Egbert, G. D.: Tides in the Weddell Sea, Ocean, Ice and Atmosphere: Interactions at the Antarctic Continental Margin, Antarct. Res. Ser, 75, 341-369, 1998.

Schwegmann, S., Haas, C., Fowler, C., and Gerdes, R.: A comparison of satellite-derived sea-ice motion with drifting-buoy data in the Weddell Sea, Antarctica, Annals of Glaciology, 52, 103-110, 10.3189/172756411795931813, 2011.

Schwegmann, S., Rinne, E., Ricker, R., Hendricks, S., and Helm, V.: About the consistency between Envisat and CryoSat-2 radar freeboard retrieval over Antarctic sea ice, Cryosphere, 9, 4893-4923, 10.5194/tc-10-1415-2016, 2016.

Spreen, G., Kaleschke, L., and Heygster, G.: Sea ice remote sensing using AMSR-E 89-GHz channels, Journal of Geophysical Research-Oceans, 113, 10.1029/2005jc003384, 2008.

Sturm, M., Holmgren, J., Konig, M., and Morris, K.: The thermal conductivity of seasonal snow, Journal of Glaciology, 43, 26-41, 1997.

Sturm, M., and Holmgren, J.: An automatic snow depth probe for field validation campaigns, Water Resources Research, 54, 9695-9701, 2018.

Thorndike, A.: A toy model linking atmospheric thermal radiation and sea ice growth, Journal of Geophysical Research: Oceans, 97, 9401-9410, 1992.

Tian, L. J., Gao, Y. L., Weissling, B., and Ackley, S. F.: Snow-ice contribution to the structure of sea ice in the Amundsen Sea, Antarctica, Annals of Glaciology, 61, 369-378, 10.1017/aog.2020.55, 2020.

Turner, J., Holmes, C., Caton Harrison, T., Phillips, T., Jena, B., Reeves-Francois, T., Fogt, R., Thomas, E. R., and Bajish, C.: Record low Antarctic sea ice cover in February 2022, Geophysical Research Letters, 49, e2022GL098904, 2022.

Venegas, S. A., and Drinkwater, M. R.: Sea ice, atmosphere and upper ocean variability in the Weddell Sea, Antarctica, Journal of Geophysical Research-Oceans, 106, 16747-16765, Doi 10.1029/2000jc000594, 2001.

Vernet, M., Geibert, W., Hoppema, M., Brown, P. J., Haas, C., Hellmer, H., Jokat, W., Jullion, L., Mazloff, M., and Bakker, D.: The Weddell Gyre, Southern Ocean: present knowledge and future challenges, Rev Geophys, 57, 623-708, 2019.

Vihma, T., Launiainen, J., and Uotila, J.: Weddell Sea ice drift: Kinematics and wind forcing, Journal of Geophysical Research: Oceans, 101, 18279-18296, https://doi.org/10.1029/96JC01441, 1996.

Webster, M., Gerland, S., Holland, M. M., Hunke, E., Kwok, R., Lecomte, O., Massom, R., Perovich, D., and Sturm, M.: Snow in the changing sea-ice systems, Nature Climate Change, 1, 2018.

Wever, N., Schmid, L., Heilig, A., Eisen, O., Fierz, C., and Lehning, M.: Verification of the multi-layer SNOWPACK model with different water transport schemes, The Cryosphere, 9, 2271-2293, 10.5194/tc-9-2271-2015, 2015.

Wever, N., Würzer, S., Fierz, C., and Lehning, M.: Simulating ice layer formation under the presence of preferential flow in layered snowpacks, The Cryosphere, 10, 2731-2744, 10.5194/tc-10-2731-2016, 2016.

Wever, N., Rossmann, L., Maaß, N., Leonard, K. C., Kaleschke, L., Nicolaus, M., and Lehning, M.: Version 1 of a sea ice module for the physics-based, detailed, multi-layer SNOWPACK model, Geoscientific Model Development, 13, 99-119, 2020.

Wever, N., Leonard, K., Maksym, T., White, S., Proksch, M., and Lenaerts, J. T.: Spatially distributed simulations of the effect of snow on mass balance and flooding of Antarctic sea ice, Journal of Glaciology, 1-19, 2021.

Willmes, S., Haas, C., Nicolaus, M., and Bareiss, J.: Satellite microwave observations of the interannual variability of snowmelt on sea ice in the Southern Ocean, Journal of Geophysical Research-Oceans, 114, 10.1029/2008jc004919, 2009.

Worby, A. P., Geiger, C. A., Paget, M. J., Van Woert, M. L., Ackley, S. F., and DeLiberty, T. L.: Thickness distribution of Antarctic sea ice, Journal of Geophysical Research-Oceans, 113, 10.1029/2007jc004254, 2008.

585